Atomic and Molecular Adsorption on Fe(110)

Lang Xu, Demetrios Kirvassilis, Yunhai Bai, Manos Mavrikakis*

Department of Chemical and Biological Engineering, University of Wisconsin-Madison, Madison, WI 53706, USA

*manos@engr.wisc.edu

Abstract

Iron is the principal catalyst for the ammonia synthesis process and the Fischer-Tropsch process, as well as many other heterogeneously catalyzed reactions. It is thus of fundamental importance to understand the interactions between the iron surface and various reaction intermediates. Here we present a systematic study of the atomic and molecular adsorption behaviors over Fe(110) using periodic, self-consistent density functional theory (DFT-GGA) calculations. The preferred binding sites, binding energies and the corresponding surface deformation energies of five atomic species (H, C, N, O, and S), six molecular species (NH_3, CH_4, N_2, CO, HCN, and NO), and eleven molecular fragments (CH, CH_2, CH_3, NH, NH_2, OH, CN, COH, HCO, NOH, and HNO) were determined on the Fe(110) surface at a coverage of 0.25 monolayer. The binding strengths calculated using the PW91 functional decreased in the following order: C > CH > N > O > S > NH > COH > CN > CH_2 > NOH > OH > HNO > HCO > NH_2 > H > NO > HCN > CH_3 > CO > N_2 > NH_3. No stable binding structures were observed for CH_4. The estimated diffusion barriers and pathways, as well as the adsorbate-surface and intramolecular vibrational modes of all the adsorbates at their preferred binding sites, were identified. Using the calculated adsorption energetics, we constructed the potential energy surfaces for a few surface reactions including the decomposition of methane, ammonia, dinitrogen, carbon monoxide and nitric oxide. These potential energy surfaces provide valuable insight into the ability of Fe(110) to catalyze common elementary steps.

Keywords: density functional theory; iron; adsorption; catalysis; diffusion.

1. Introduction

The application of metallic iron as a heterogeneous catalyst lies at the heart of two extremely important industrial catalytic processes: the Haber–Bosch process for ammonia synthesis and the Fischer-Tropsch process for conversion of syngas to hydrocarbon fuels. The process of ammonia synthesis from nitrogen and hydrogen is one of the most studied heterogeneously catalyzed reactions [1]. Among transition metals, Fe and Ru have been shown to be the best monometallic catalysts for ammonia synthesis [2–4]. Numerous research studies have been conducted to elucidate the reaction mechanism and the nature of active sites for the ammonia synthesis reaction over iron catalysts [5–20]. The Fischer-Tropsch process allows the production of hydrocarbon fuels from alternative resources other than petroleum crude oil. Since the strong C–O bond in carbon monoxide needs to be activated in the Fischer-Tropsch process, a highly active catalytic surface such as Fe or Co is often required for this chemistry [21,22]. The Fischer-Tropsch mechanism over iron catalysts has been extensively studied in the literature both experimentally [23–32] and theoretically [32–34]. A detailed review of the mechanisms of iron-catalyzed reactions is beyond the scope of this paper. Interested readers are directed to the references herein. Due to the significant relevance of iron catalysts in industrial applications, fundamental understanding of the adsorption behavior of different atomic and molecular reactive intermediates over the iron surface has been the topic of many surface science research studies.

Here we focus on the Fe(110) surface, the most stable facet of this body-centered cubic metal. Atomic species such as H, C, N, O, and S are ubiquitously present in catalytic reactions. Additionally, C, N, O, and S are common impurities that naturally exist in metallic iron [35]. The adsorption of H on Fe(110) has been extensively characterized using experimental techniques such as electron energy loss spectroscopy (EELS) [36], low electron energy diffraction (LEED) [37–43], thermal desorption spectroscopy (TDS) [37,39,42,44], ultraviolet photoelectron spectroscopy (UPS) [42], and thermal energy atom scattering (TEAS) [44], as well as theoretical methods such as the tight-binding method (TB) [45] and density functional theory (DFT) [46,47]. N adsorption on Fe(110) has been studied using LEED [48,49], UPS [48,49], temperature-programmed desorption (TPD) [49,50], work function measurements [51], helium atom scattering (HAS) [52], and DFT [53–55]. Numerous studies have been performed on the adsorption of O on Fe(110), including LEED [48,56–63], UPS, X-ray photoelectron spectroscopy (XPS) [62,64], angle-

resolved photoelectron spectroscopy (ARPES) [60,65,66], EELS, scanning tunneling microscopy (STM) [57,64], X-ray absorption spectroscopy (XAS) [63], and DFT [67–69]. Surface science studies of C and S adsorption on Fe(110) are relatively scarce: adsorption of C has been studied using LEED [35,48,70], UPS [48], and DFT [71–73]; S adsorption on Fe(110) has been studied using LEED [35,48,74–76], UPS [48], STM [74], and DFT [77,78]. Besides the atomic species, adsorption properties of molecules such as NH_3 and CO are also common topics in surface science studies on Fe(110). Adsorption of NH_3 on Fe(110) has been studied using techniques such as LEED [37,79,80], HAS [81], secondary ion mass spectroscopy (SIMS) [79], AES [82], TDS [37,80], work function measurements [80], EELS [83,84], and DFT [85]. Numerous research work has been conducted on the adsorption of CO on Fe(110); to list a few, studies have been performed using LEED [37,48,86–89], HAS [81], TDS [37,90,91], UPS [48,87,92,93], XPS [87], EELS [88], work function measurements [94], ARPAS [95], and DFT [96–99].

In this work, we seek to construct a comprehensive, self-consistent, first-principles based database of adsorption properties, diffusion behavior and vibrational features of atomic and molecular species over Fe(110). The experimental identification and measurement of molecular fragments such as CH_x and NH_x can often be challenging tasks. Additionally, computational studies are often conducted using different methods and parameterizations, which makes it difficult to compare and generalize results from different sources. In the past, our group has conducted similar work on a number of other close-packed transition metal surfaces, including Rh(111) [100], Ir(111) [101], Pt(111) [102], Pd(111) [103], Ru(0001) [104], Re(0001) [105] and Au(111) [106]. Here we performed periodic, self-consistent DFT calculations to study the adsorption of a total of 22 atoms, molecules and molecular fragments commonly involved in Fe-catalyzed reactions, and we compare our results to experimental data as available. Using our calculated binding energy values, we also constructed potential energy surfaces for the thermochemistry of several surface reactions, which are relevant in the activation processes of NH_3, CH_4, N_2, CO, and NO on Fe catalysts. These DFT-derived results present a set of benchmarks that can be used for comparison with experiments, including state-of-the-art single crystal adsorption microcalorimetry [107,108]. Our data can also be added to other electronically accessible databases, which have started appearing recently [109].

2. Methods

DACAPO, a planewave, total energy code [110,111], was used for all the spin-polarized DFT calculations in this work. The Kohn-Sham one-electron valence states were expanded in a plane wave basis set with kinetic energies below 25 Ry [110], and the ionic cores were represented by ultrasoft pseudopotentials [112]. The self-consistent GGA-PW91 functional [113] was used to describe the exchange-correlation energy. Energies obtained using the RPBE functional [110], not self-consistently, were also reported. Throughout the text, the RPBE energies are listed in square brackets, next to PW91 values. The self-consistent electron densities were determined by iterative diagonalization of the Kohn-Sham Hamiltonian, Fermi-population of the Kohn-Sham states (k_BT = 0.1 eV) and Pulay mixing of the resulting electron densities [114]. All total energies were extrapolated to (k_BT = 0 eV) [110]. The first Brillouin zone was sampled by a (6 × 6 × 1) Monkhorst-Pack k-point mesh [115]. Convergence with respect to calculation parameters has been ensured up to 0.05 eV.

The Fe(110) surface was modeled by a four-layer slab periodically repeated in a supercell geometry consisting of a (2 × 2) unit cell, which corresponds to a surface coverage of 0.25 monolayer (ML) if a single adsorbate is present in the unit cell. The top two layers of the metal atoms, as well as all the adsorbate atom(s), were fully relaxed, while the bottom two layers of the slab were fixed at their bulk-truncated lattice positions. In the vertical direction along the surface norm, a vacuum layer of at least five equivalent atomic layers (~11 Å) in thickness was added between any two successive slabs, so that the adsorbate-surface interactions were not influenced by any surface atoms from the neighboring unit cells. Adsorption was allowed on only one side of the two exposed surfaces of each slab, and the electrostatic potential was adjusted accordingly [116,117]. The calculated lattice constant for Fe using the PW91 functional is 2.850 Å, in close agreement with the experimental value of 2.866 Å [118]. The Fe(110) slab used in all the calculations is illustrated in Figure 1. Four types of high-symmetry binding sites exist on the (110) plane: top, long-bridge (lb), short-bridge (sb) and 3-fold hollow (h). Such a naming convention is used throughout the subsequent discussion.

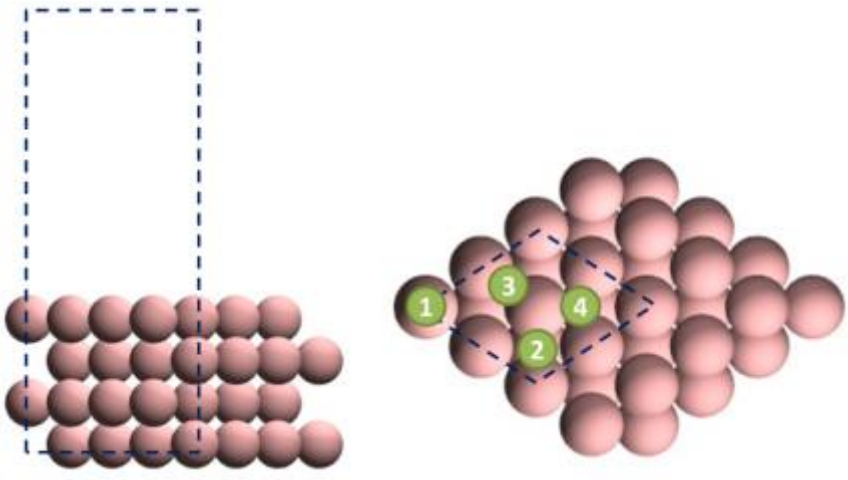

Figure 1: Side (left) and top (right) views of a clean Fe(110) slab. The dashed lines denote the (2 × 2) unit cell**.** The numbers indicate the locations of the four high-symmetry binding sites on Fe(110): 1 – top, 2 – long bridge (lb), 3 – short bridge (sb), and 4 – hollow (h).

The binding energy (E_b) of an adsorbate is defined using Equation (1):

$$E_b = E_{\text{total}} - E_{\text{substrate}} - E_{\text{gas-phase adsorbate}} \quad (1)$$

where E_{total} is the total energy of the entire adsorbate-slab system, $E_{\text{substrate}}$ is the total energy of the clean Fe(110) slab by itself, and $E_{\text{gas-phase adsorbate}}$ is the total energy of the isolated adsorbate in the gas phase. By this definition, exothermic adsorption is indicated by a negative BE value; i.e., a more negative E_b value is associated with enhanced binding strength. The deformation energy of the surface upon the adsorption of a certain species (ΔE) is defined using Equation (2):

$$\Delta E = E_{\text{total, adsorbate removed}} - E_{\text{substrate}} \quad (2)$$

where $E_{\text{total, adsorbate removed}}$ is the total energy of the clean slab in which all the atoms are fixed at their corresponding positions after adsorption. This quantity is generally positive, which indicates the energy required for the surface deformation in order to accommodate the adsorption event. The electronic contribution to the adsorbate-surface interaction can thus be estimated by subtracting ΔE from E_b.

Vibrational analyses were performed by diagonalizing the mass-weighted Hessian Matrix, and the second derivatives of the total energy were evaluated using a finite difference approach with a step size of 0.010 Å [119], so that the harmonic vibrational frequencies were obtained. The diffusion barrier of an adsorbate was estimated by first constructing a probable diffusion path between two

adjacent energy minima on the potential energy surface (PES) through a metastable state and then calculating the energy difference between the most stable and the metastable states.

3. Results

In this section, we present and discuss the adsorption behavior for a total of 20 species including atoms, molecules and molecular fragments on Fe(110). The binding energy and site preference of each adsorbate are listed in Tables 1 and 2, with the detailed structural information at each preferred binding site summarized in Figure 2 and Table 3. The diffusion behavior and surface deformation energies are listed in Tables 4 and 5, respectively. The adsorption of strongly bound species (e.g., C and CH) are generally associated with large deformation energies and estimated diffusion barriers; however, we did not observe any explicit correlation between binding energy and deformation energy/diffusion barrier. The vibrational features of the adsorbates are summarized in Tables 6, 7 and 8. In the end, we present the thermochemical potential energy surfaces of a few surface reactions relevant in industrial catalysis (Figures 4 and 5).

Table 1: Binding energies (PW91 [RPBE]) and site preferences of atomic species on Fe(110)

Adsorbate	**Preferred site**		**Binding energy (eV)**[a,b]				
	Calc.	Exp.	top	long bridge	hollow	Exp.	
H	hollow	hollow[c] lb[d]	-2.25 [-2.11]		**-3.02 [-2.86]**	-2.88 0.05[e]	±
C	lb		-5.23 [-4.83]	**-7.60 [-6.99]**			
N	lb		-3.97 [-3.61]	**-6.15 [-5.57]**		-5.98[f]	
O	lb	lb[g]	-4.46 [-3.99]	**-6.09 [-5.48]**	-6.09 [-5.46]		
S	lb	lb[h]	-4.35 [-3.98]	**-5.72 [-5.22]**			

[a] No stable binding structures were found on short bridge sites.
[b] The binding energy of the most stable site (according to the PW91 binding energies) for each species is boldfaced.
[c] LEED [38,40,41]
[d] LEED [42,43]
[e] H_2, TDS [44]
[f] N_2, TPD [50]
[g] EELS [61], STM [57]
[h] STM [74]

Table 2: Binding energies (PW91 [RPBE]) and site preferences of molecules and molecular fragments on Fe(110)

Adsorbate	**Preferred Site**		**Binding Energy (eV)**[a]				
	Calc.	Exp.	top	long bridge	short bridge	hollow	Exp.
NH_3	top	lb[b]	**-0.62 [-0.30]**				-0.74[c]

CO	lb	top[d]	-1.91 [-1.58]	**-1.93** **[-1.52]**		-1.88 [-1.51]
HCN	h-lb-h		-0.63 [-0.19]		-0.59 [-0.10]	**-2.49** **[-1.79]** **(h-lb-h)** -2.27 [-1.56] (h-sb-h)
N_2	top		**-0.63** **[-0.24]**	-0.22 [0.24]		
NO	hollow		-2.59 [-2.08]	-2.84 [-2.23]	-2.71 [-2.13]	**-2.86** **[-2.24]**
CH	lb		-5.24 [-4.72]	**-6.85** **[-6.24]**		
CH_2	hollow		-3.18 [-2.74]	-4.27 [-3.70]		**-4.32** **[-3.75]**
CH_3	hollow		-1.59 [-1.27]			**-2.09** **[-1.60]**
NH	lb		-3.25 [-2.76]	**-5.22** **[-4.60]**		
NH_2	lb		-2.43 [-1.99]	**-3.03** **[-2.46]**	-2.97 [-2.42]	
OH	hollow		-3.09 [-2.46]			**-3.81** **[-3.21]**
CN	h-lb-h		-3.62 [-3.29]	-4.74 [-4.19] (lb-top) -4.27 [-3.83]		**-5.04** **[-4.40]** **(h-lb-h)**
COH	lb		-3.62 [-3.10]	**-4.75** **[-4.15]**	-4.40 [-3.82]	
HCO	h-lb-h		-2.75 [-2.15] (t-lb-t)			**-3.06** **[-2.40]** **(h-lb-h)**
NOH	lb			**-3.98** **[-3.26]**		
HNO	sb-lb-sb		-2.91 [-2.28] (t-lb-t)	**-3.61** **[-2.81]** **(sb-lb-sb)**		-3.20 [-2.49] (h-lb-h)

[a] The binding energy of the most stable site (according to the PW91 binding energies) for each species is boldfaced.
[b] LEED [80]
[c] TDS [80]
[d] LEED [88]

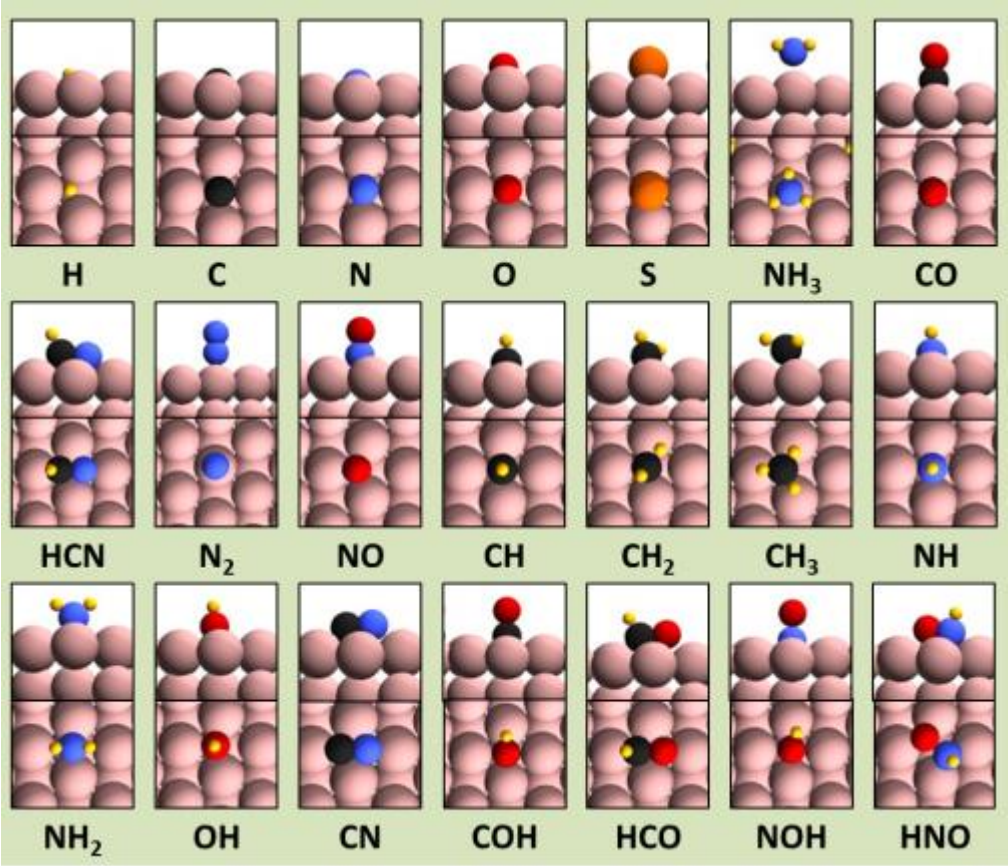

Figure 2: Side (top) and top views (bottom) of the most stable binding structures of adsorbates on Fe(110). Color Code: yellow – hydrogen, black – carbon, blue – nitrogen, red – oxygen, orange – sulfur, pink – iron.

Table 3: Geometry of the adsorbates at their preferred sites on Fe(110)

Adsorbate	$Z_{A–Fe}$ **(Å)**[a]	ΔZ_{Fe} **(Å)**[a]	$d_{Fe–Fe}$ **(Å)**[a, b]	$d_{A–B}$ **(Å)**[a]
H (hollow)	0.948	0.004	2.856 (lb)	
			2.478 (sb)	
C (lb)	0.617	-0.033	3.363 (lb)	
			2.525 (sb)	
N (lb)	0.664	-0.016	3.328 (lb)	
			2.508 (sb)	
O (hollow)	1.058	-0.014	3.074 (lb)	
			2.488 (sb)	
S (lb)	1.572	-0.054	3.071 (lb)	
			2.493 (sb)	
NH_3 (top)	2.155	0.173	2.859 (lb)	1.027 (N–H)
			2.479 (sb)	
CO (lb)	1.312	-0.037	2.951 (lb)	1.211 (C–O)
			2.454 (sb)	
HCN (h-lb-h)	1.423 (C–Fe)	-0.015	2.910 (lb)	1.328 (C–N)
	1.300 (N–Fe)		2.499 (sb)	1.102 (C–H)
N_2 (top)	1.842	0.020	2.852 (lb)	1.142 (N–N)
			2.468 (sb)	

NO (hollow)	1.193	0.009	2.853 (lb) 2.496 (sb)	1.242 (N–O)
CH (lb)	1.081	-0.039	3.094 (lb) 2.465 (sb)	1.106 (C–H)
CH_2 (hollow)	1.255	-0.009	2.981 (lb) 2.473 (sb)	1.176, 1.104 (C–H)
CH_3 (hollow)	1.604	0.007	2.831 (lb) 2.473 (sb)	1.118 (C–H)
NH (lb)	1.059	-0.024	3.129 (lb) 2.477 (sb)	1.030 (N–H)
NH_2 (lb)	1.422	0.060	2.869 (lb) 2.518 (sb)	1.032 (N–H)
OH (hollow)	1.311	0.014	3.030 (lb) 2.512 (sb)	0.981 (O–H)
CN (h-lb-h)	1.426 (N–Fe) 1.295 (C–Fe)	-0.007	2.947 (lb) 2.510 (sb)	1.260 (C–N)
COH (lb)	1.150	-0.038	3.048 (lb) 2.462 (sb)	1.362 (C–O) 0.987 (O–H)
HCO (h-lb-h)	1.552 (O–Fe) 1.398 (C–Fe)	-0.013	2.994 (lb) 2.492 (sb)	1.345 (C–O) 1.107 (C–H)
NOH (lb)	1.028	-0.031	3.164 (lb) 2.480 (sb)	1.440 (N–O) 0.990 (O–H)
HNO (sb-lb-sb)	1.519 (O–Fe) 1.371 (N–Fe)	-0.013	3.145 (lb) 2.493 (sb)	1.473 (N–O) 1.030 (N–H)

[a] The parameter definitions are provided in Figure 3.

[b] On the clean, relaxed Fe(110) surface, $d_{Fe–Fe}$ values are 2.850 Å along the long-bridge direction and 2.468 Å along the short-bridge direction.

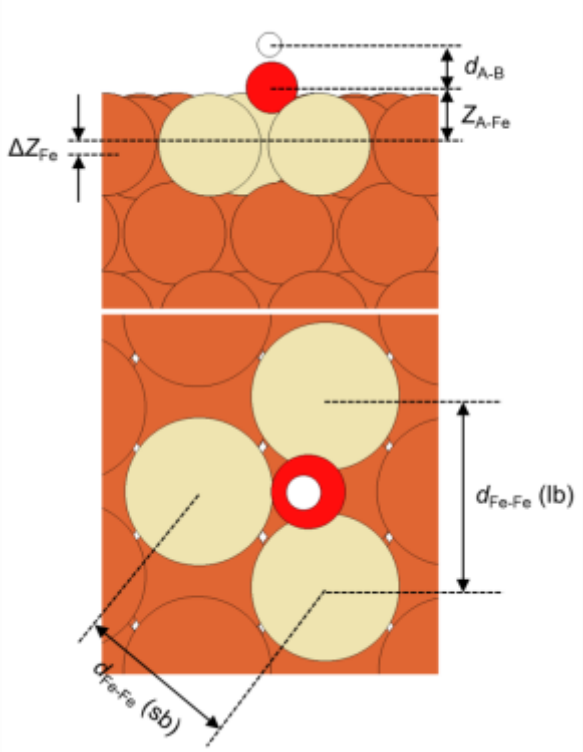

Figure 3: Definitions of the geometric parameters for surface adsorbates. Side (top) and top (bottom) views of an adsorbate on the Fe(110) slab are shown. $Z_{A–Fe}$ denotes the vertical distance between the adsorbate and the plane of the Fe atoms in contact with it (the highlighted slab atoms). ΔZ_{Fe} denotes the average difference in vertical distances between the plane of the highlighted Fe atoms and that of a clean, relaxed Fe(110) surface. ΔZ_{Fe} is positive when the highlighted atoms are pulled upwards, and *vice versa*. $d_{Fe–Fe}$ denotes the average distance between adjacent Fe atoms in contact with the adsorbate. Two $d_{Fe–Fe}$ values were evaluated: one along the long-bridge direction (denoted by lb) and the other along the short-bridge direction (denoted by sb). On a clean, relaxed Fe(110) surface, $d_{Fe–Fe}$ values are 2.850 Å (lb) and 2.468 Å (sb), respectively. $d_{A–B}$ denotes the intramolecular bond length of the adsorbate.

Table 4: Estimated diffusion barriers and paths for adsorbates on Fe(110)

Adsorbate	**Diffusion barrier (eV)**		**Diffusion path**
	PW91	RPBE	
H	0.18	0.21	hollow→sb[b]→hollow
C	1.21	1.12	lb→sb[b]→lb
N	0.86	0.78	lb→sb[b]→lb
O	0.40	0.38	lb→sb[b]→lb
S	0.61	0.59	lb→sb[b]→lb
NH_3	0.28	0.31	top→sb[b]→top
CO	0.02	0.04	lb→top→lb
HCN	0.22	0.22	h-lb-h→h-sb-h→h-lb-h
N_2	0.24	0.28	top→hollow[a]→top
NO	0.02	0.01	hollow→lb→hollow
CH	0.68	0.68	lb→sb[b]→lb
CH_2	0.05	0.04	hollow→lb→hollow
CH_3	0.17	0.17	hollow→lb[a]→hollow
NH	0.70	0.69	lb→sb[b]→lb
NH_2	0.35	0.37	lb→hollow[a]→sb

OH	0.11	0.12	hollow→lb[b]→hollow
CN	0.30	0.20	h-lb-h→lb-top→h-lb-h
COH	0.35	0.34	lb→sb→lb
HCO	0.31	0.24	h-lb-h→t-lb-t→h-lb-h
NOH	0.63	0.61	lb→sb[b]→lb
HNO	0.41	0.31	sb-lb-sb→h-lb-h→sb-lb-sb

[a] The energy of the adsorbate at the metastable site was calculated by fixing the x and y coordinates of the atom through which the adsorbate binds to the slab.
[b] The energy of the adsorbate at the metastable site was calculated by fixing the x and y coordinates of the atom through which the adsorbate binds to the slab, as well as all the slab atoms.

Table 5: Deformation energies upon adsorption of the adsorbates at their preferred sites on Fe(110)

Adsorbate	**Site**	**Δ*E* (eV)**	
		PW91	RPBE
H	hollow	0.00	0.00
C	lb	0.32	0.34
N	lb	0.28	0.28
O	hollow	0.05	0.06
S	lb	0.07	0.08
NH_3	top	0.08	0.07
CO	lb	0.04	0.04
HCN	h-lb-h	0.03	0.04
N_2	top	0.02	0.03
NO	hollow	0.02	0.03
CH	lb	0.09	0.09
CH_2	hollow	0.03	0.03
CH_3	hollow	0.02	0.03
NH	lb	0.10	0.10
NH_2	lb	0.08	0.10
OH	hollow	0.05	0.06
CN	h-lb-h	0.05	0.05
COH	lb	0.07	0.06
HCO	h-lb-h	0.04	0.05
NOH	lb	0.12	0.12
HNO	sb-lb-sb	0.12	0.13

Table 6: Vibrational frequencies of atomic adsorbate species at their most stable binding sites on Fe(110)

Adsorbate	**Frequency (cm^{-1})**	
	Calc.	Expr.
H	1056	1060[a]
C	371	
N	359	
O	488	500[b]
S	331	

[a] EELS [36]
[b] EELS [61]

Table 7: Vibrational frequencies of diatomic adsorbate species at their most stable binding sites on Fe(110)

Adsorbate	**Calculated (cm^{-1})**		**Experimental (cm^{-1})**	
	IM	AS	IM	AS
CO	1752	314	1890[a]	456[a]
N_2	2158	329		
NO	1464	340		
CH	2984	524		
NH	3424	495		
OH	3794	380		
CN	1590	342		

IM stands for intramolecular; AS stands for adsorbate-surface.
[a] EELS [88]

Table 8: Vibrational frequencies of polyatomic adsorbate species at their most stable binding sites on Fe(110)

Adsorbate	**Calculated Frequency (cm^{-1})**						
	Symm. IM	Asymm. IM	AS	Scissoring	Rocking	Wagging	Twisting
NH_3	3370	3525	277	1544	461	1027	50.2
		3527		1552	463		
HCN		1320[a]	417.9	1041	450.8	735.4	246
		3003[b]					
CH_2	2241	3002	464	1359	524	699	298
CH_3	2763	2805	335	1292	525	1182	377
		2892		1297	455		
NH_2	3355	3429	404	1485	503	606	432
COH		1100[c]	359	1188	290		235
		3692[d]			427		
HCO		1127[c]	298	1182	463	717	138
		2950[b]					
NOH		798[e]	331	1253	303		171
		3663[d]			493		
HNO		667[e]	416	1205	471	583	341
		3432[f]					

Symm. IM stands for symmetric intramolecular; asymm. IM stands for asymmetric intramolecular; AS stands for adsorbate-surface.
[a] ν(C–N)
[b] ν(C–H)
[c] ν(C–O)
[d] ν(O–H)
[e] ν(N–O)
[f] ν(N–H)

3.1 Adsorption of Atomic Species

3.1.1 Hydrogen (H)

H prefers to bind to the hollow site of Fe(110), with a binding energy of -3.02 [-2.86] eV (Figure 2 and Table 1). Our predicted optimal binding site for H agrees with the LEED studies by Hammer et al. [41], Moritz et al. [40], and Nichtl-Pecher et al. [38], though earlier experimental studies suggested H binding on the long bridge site [42,43]. The calculated binding energy is in good agreement with the experimental value of -2.88 ± 0.05 eV estimated from TDS [44]. H can also bind on a top site, with a much lower binding energy of -2.25 [-2.11] eV. H is the least strongly bound among all the atomic species studied in this work. At its preferred binding site, the H atom sits 0.948 Å above the surface. The adsorption of H barely causes any distortion to the Fe(110) surface; we obtained a negligible deformation energy associated with the adsorption event (Table 5). The calculated H-Fe stretching mode is at 1056 cm^{-1} (Table 6), in excellent agreement with the experimental HREELS value of 1060 cm^{-1} [36]. H prefers to diffuse on Fe(110) from a hollow site to the adjacent hollow site through the short bridge site in between, and the estimated energy barrier for this diffusion path is 0.18 [0.21] eV (Table 4).

3.1.2 Carbon (C)

The preferred binding site for C on Fe(110) is the long bridge site with a binding energy of -7.60 [-6.99] eV (Figure 2 and Table 1). Carbon is the most strongly bound adsorbate among all the species evaluated. We also found a stable adsorption structure for C on the top site; however, the binding strength is much weaker (-5.23 [-4.83] eV). Over its preferred long bridge site, the carbon atom lies 0.617 Å above the Fe(110) surface (Table 3). The adsorbate-surface stretching frequency is 371 cm^{-1} (Table 6). The adsorption of C on the long bridge site creates a significant distortion of the surface: it pushes the two adjacent Fe atoms away by 0.513 Å and downwards by 0.033 Å (Table 3). Therefore, the adsorption is associated with a notable deformation energy of 0.32 [0.34] eV (Table 5). The optimal diffusion path for C on Fe(110) is long bridge → short bridge → long bridge, and the estimated diffusion barrier is 1.21 [1.12] eV (Table 4). Sahputra *et al.* calculated the diffusion barrier for C on Fe(110) using DFT and the nudged elastic band (NEB) method [120]. Our estimated diffusion barrier is in excellent agreement with their reported value of 1.08 eV.

3.1.3 Nitrogen (N)

As shown in Table 1, N can bind on either the long bridge (E_b = -6.15 [-5.57] eV) or top (E_b = -3.97 [-3.61] eV) site of the Fe(110) surface. The PW91 binding energy value at the long bridge site is

in reasonable agreement with the experimentally estimated value of -5.98 eV (TPD [50]). Its preferred long bridge binding structure is illustrated in Figure 2, where the N atom is adsorbed at a vertical distance of 0.664 Å from the surface (Table 3). The calculated N-surface stretching mode in this binding structure is at 359 cm^{-1} (Table 6). Similar to the adsorption of C, N adsorption leads to large displacements of the surface Fe atoms; upon its adsorption, the two adjacent surface Fe atoms are driven farther apart by 0.478 Å (Table 3), which is associated with a notable deformation energy of 0.28 [0.28] eV (Table 5). Along the preferred diffusion path for N on Fe(110), the atom moves between two adjacent long bridge sites through a short bridge site, climbing over an estimated barrier of 0.86 [0.78] eV (Table 4).

3.1.4 Oxygen (O)

O prefers to bind on the long bridge site of the Fe(110) surface with a binding energy of -6.09 [-5.48] eV; the hollow site is almost isoenergetic (E_b = -6.09 [-5.46] eV). A less energetically favorable binding structure exists over the top site with a binding energy of -4.46 [-3.99] eV (Figure 2 and Table 1). Experimental observations suggest that O binds to the long bridge site at a surface coverage of ~0.25 ML [57,61], consistent with our calculation results. At its preferred long bridge site, the O atom lies at a vertical distance of 1.058 Å from the surface (Table 3), and the calculated O-Fe stretching frequency is 488 cm^{-1} (Table 6). This frequency value is in good agreement with the EELS result (500 cm^{-1}) obtained by Erley and Ibach [61]. The adsorption of an O atom leads to moderate distortion of the Fe surface atoms: the adjacent surface atoms are pushed downwards by 0.014 Å, and the local lattice is slightly expanded by 0.224 Å and 0.020 Å, in the long-bridge and short-bridge directions, respectively (Table 3). O adsorption is therefore accompanied by a mild deformation energy value of 0.05 [0.06] eV (Table 5). The oxygen can diffuse between two adjacent long bridge sites through a short bridge site; such a diffusion path is associated with an estimated energy barrier of 0.40 [0.38] eV (Table 4).

3.1.5 Sulfur (S)

Atomic sulfur can bind on either the long bridge (E_b = -5.72 [-5.22] eV) or top (E_b = -4.35 [-3.98] eV) site of the Fe(110) surface (Table 1). Our predicted preferred binding site of S (long bridge) agrees well with the STM results by Weissenrieder et al. [74]. When S binds to its preferred adsorption site (long bridge, Figure 2), the adsorbate atom sits at a vertical distance of 1.572 Å

from the surface (Table 3). The calculated adsorbate-surface vibrational mode is at 331 cm^{-1} (Table 6). Upon the adsorption of a sulfur atom, the adsorbate pushes the adjacent surface Fe atoms down by 0.054 Å and farther apart by 0.221 Å (Table 3); we obtained a deformation energy value of 0.07 [0.08] eV (Table 5). The optimal diffusion path of S on Fe(110) is long bridge → short bridge → long bridge, and the diffusion barrier is estimated to be 0.61 [0.59] eV (Table 4).

3.2 Adsorption of Molecules or Molecular Fragments

Here we continue to discuss the adsorption of molecules and molecular fragments on Fe(110). We did not observe any stable binding structure for methane (CH_4). The result is expected since CH_4 is a closed-shell species which interacts with most surfaces only through weak physical interactions, not accounted for in this study. We will present the detailed adsorption behavior of the rest of molecular species and fragments in the following sections.

3.2.1 Ammonia (NH_3)

We observed only one stable binding site on Fe(110) for ammonia: the top site, and the binding is the weakest among all the adsorbates studied except CH_4 (E_b = -0.62 [-0.30] eV) (Figure 2 and Table 2). The calculated binding energy is in reasonable agreement with the TDS-estimated value of -0.74 eV [80]; LEED results from the same work, however, suggest that NH_3 binds on the long bridge site. The NH_3 molecule sits at a relatively large vertical distance of 2.155 Å from the surface, consistent with its weak adsorption strength. The intramolecular N–H bond length is 1.027 Å (Table 3). The calculated vibrational modes of adsorbed NH_3 are summarized in Table 8: we obtained one symmetric N–H stretching mode at 3370 cm^{-1} and two asymmetric N–H modes at 3525 cm^{-1} and 3527 cm^{-1}. Upon adsorption of NH_3 on Fe(110), the adsorbed molecule pulls the adjacent surface atom upwards by 0.173 Å (Table 3), which is associated with a deformation energy of 0.08 [0.07] eV (Table 5). The NH_3 molecule prefers to diffuse between adjacent top sites through the short bridge site in the middle; such a diffusion path has an estimated energy barrier of 0.28 [0.31] eV (Table 4).

3.2.2 Carbon Monoxide (CO)

As summarized in Table 2, CO can bind on three of the four high-symmetry sites on Fe(110) with very similar binding energies; the PW91 binding strength decreases in the order of long bridge (E_b

= -1.93 [-1.52] eV) > top (E_b = -1.91 [-1.58] eV) > hollow (E_b = -1.88 [-1.51] eV). Using LEED and EELS, Erley reported that CO binds on the top site of the Fe(110) surface at low coverage [88], which contradicts our PW91 result but corroborates the RPBE functional prediction. It is a known issue that the PW91 functional tends to favor binding of CO at higher-coordination sites at different metal surfaces [121,122], and therefore it does not work well in predicting the preferred binding site for CO. Over its preferred long bridge binding site (Figure 2), the CO molecule is adsorbed 1.312 Å above the surface and the C–O bond length is 1.211 Å (Table 3). The calculated C–O and Fe–CO stretching frequencies of CO on the long bridge site are 1752 cm^{-1} and 314 cm^{-1}, respectively (Table 7). The calculated frequencies are underestimates compared with the experimental EELS values of 1890 cm^{-1} and 456 cm^{-1} [88], likely due to the differences in CO binding sites and CO coverage between experiment and theory. Similar results were reported by Stibor et al. [97] in their DFT calculations, where the calculated frequency values are also significantly lower than the experimental ones. The adsorption of CO leads to mild surface deformation with an energy value of 0.04 [0.04] eV (Table 5). Along its preferred diffusion path over Fe(110), the CO molecule moves from a long bridge site to the adjacent one through a top site, which is associated with an estimated diffusion barrier of merely 0.02 [0.04] eV (Table 4).

3.2.3 Hydrogen Cyanide (HCN)

The HCN molecule prefers to bind through both the carbon and nitrogen atoms on the Fe(110) surface. In its most stable binding structure, both the C and N atoms bind on a pair of adjacent hollow sites across a long bridge site in an h-lb-h geometry as illustrated in Figure 2 (E_b = -2.49 [-1.79] eV, Table 2). The molecule binds in a less energetically favorable structure over two adjacent hollow sites across a short bridge site (h-sb-h, E_b = -2.27 [-1.56] eV). The adsorption structure through a single N atom in a vertical orientation over the top or short bridge site is much less stable, as summarized in Table 2 (E_b (top) = -0.63 [-0.19] eV; E_b (sb) = -0.59 [-0.10] eV). In its most stable h-lb-h configuration, the C and N atoms are located at vertical distances of 1.423 Å and 1.300 Å, respectively, from the Fe(110) surface; the intramolecular C–N and C–H bond lengths are 1.328 Å and 1.102 Å, respectively (Table 3). The adsorption of HCN is associated with mild surface deformation (0.03 [0.04] eV in energy, Table 5). The optimal diffusion path of HCN on Fe(110) is h-lb-h → h-sb-h → h-lb-h, and the estimated diffusion barrier associated with this path is 0.22 [0.22] eV (Table 4).

3.2.4 Dinitrogen (N_2)

The most stable binding structure of the dinitrogen molecule is illustrated in Figure 2. The molecule binds vertically over a top site through one of the two N atoms (E_b = -0.63 [-0.24] eV). It binds weaker on the long bridge site with a binding energy of -0.22 [0.24] eV (Table 2). Over the top site on Fe(110), the N_2 molecule lies 1.842 Å vertically away from the surface, and the intramolecular N–N bond distance is 1.142 Å (Table 3). The calculated intramolecular and adsorbate-surface stretching modes of adsorbed N_2 are at 2158 cm^{-1} and 329 cm^{-1}, respectively (Table 7). The adsorption of N_2 on Fe(110) causes a mild surface deformation of 0.02 [0.03] eV in energy (Table 5). On its optimal diffusion path, the N_2 molecule diffuses from one top site to the adjacent top site through a hollow site, which is associated with an estimated energy barrier of 0.24 [0.28] eV (Table 4).

3.2.5 Nitric Oxide (NO)

Similar to CO, the nitric oxide molecule can bind stably on all the four high-symmetry sites on Fe(110). The PW91 binding strength decreases in the order of hollow (E_b = -2.86 [-2.24] eV) > long bridge (E_b = -2.84 [-2.23] eV) > short bridge (E_b = -2.71 [-2.13] eV) > top (E_b = -2.59 [-2.08] eV) (Table 2). The NO molecule is adsorbed at a vertical distance of 1.193 Å above its preferred hollow site, with the N atom closer to the surface, and the N–O bond length at 1.242 Å (Table 3). The calculated vibrational features of adsorbed NO are summarized in Table 7; the intramolecular and adsorbate-surface stretching frequencies are 1464 cm^{-1} and 340 cm^{-1}, respectively. The adsorption of NO is associated with rather an insignificant surface distortion with a deformation energy of 0.02 [0.03] eV (Table 5). NO prefers to diffuse over Fe(110) between two adjacent hollow sites through the long bridge site in between; the estimated diffusion barrier for this path is merely 0.02 [0.01] eV (Table 4).

3.2.6 Methylidyne (CH), Methylene (CH_2) and Methyl (CH_3)

The CH species prefers to bind on the long bridge site on Fe(110), while both CH_2 and CH_3 prefer to bind on the hollow sites (Figure 2). The binding strength at the preferred site of each decreases with increasing number of hydrogen atoms: CH (E_b = -6.85 [-6.24] eV) > CH_2 (E_b = -4.32 [-3.75] eV) > CH_3 (E_b = -2.09 [-1.60] eV) (Table 2). The detailed adsorption geometries of CH, CH_2, and CH_3 at their preferred adsorption sites are summarized in Table 3. CH is adsorbed at a vertical

distance of 1.081 Å from the surface, and the intramolecular C–H bond distance is 1.106 Å. CH_2 lies 1.255 Å above the surface in a bent structure, in which one H atom is closer to the surface than the other; the two C–H bond distances are 1.176 Å and 1.104 Å. CH_3 is adsorbed in an upright orientation 1.604 Å above the surface; all three C–H bonds have approximately the same length of 1.118 Å. We calculated the surface vibrational modes for each CH_x species at its preferred site. The C–H and Fe–CH stretching frequencies of surface CH are 2984 cm^{-1} and 524 cm^{-1}, respectively (Table 7). The calculated surface vibrational modes of CH_2 and CH_3 are summarized in Table 8: the symmetric C–H stretching modes in CH_2 and CH_3 are at 2241 cm^{-1} and 2763 cm^{-1}, respectively; CH_2 has one asymmetric C–H stretching mode at 3002 cm^{-1} and CH_3 has two asymmetric C–H stretching modes at 2805 cm^{-1} and 2892 cm^{-1}. CH causes the strongest degree of surface deformation (0.09 [0.09] eV in energy) upon adsorption on Fe(110) among the three CH_x species, which is mostly due to the horizontal expansion of the neighboring surface Fe atoms by 0.244 Å. The surface deformations associated with CH_2 and CH_3 adsorption are rather insignificant (0.03 [0.03] eV and 0.02 [0.03] eV in energy, respectively) (Table 5). We estimated the surface diffusion paths and barriers of the CH_x species as summarized in Table 4. CH diffuses between two adjacent long bridge sites through a short bridge site with an energy barrier 0.68 [0.68] eV. Both CH_2 and CH_3 diffuse between two adjacent hollow sites through the long bridge site in the middle; the estimated diffusion barriers of CH_2 and CH_3 are 0.05 [0.04] eV and 0.17 [0.17] eV, respectively.

3.2.7 Imide (NH) and Amide (NH_2)

Both NH and NH_2 prefer to bind on the long bridge sites on Fe(110), with binding energies of -5.22 [-4.60] eV and -3.03 [-2.46] eV, respectively (Figure 2 and Table 2). Table 3 summarizes the detailed adsorption geometries of NH and NH_2 at their preferred binding sites. NH is adsorbed at a vertical distance of 1.059 Å from the surface, and the calculated intramolecular N–H bond length is 1.030 Å. NH_2 sits 1.422 Å above the surface, and the calculated N–H bond length is 1.032 Å. The calculated N–H and Fe–NH vibrational modes of NH are at 3424 cm^{-1} and 495 cm^{-1}, respectively (Table 7); the calculated symmetric and asymmetric N–H stretching frequencies of NH_2 are 3355 cm^{-1} and 3429 cm^{-1}, respectively (Table 8). The adsorption of NH and NH_2 is associated with similar deformation energies (0.10 [0.10] eV and 0.08 [0.10] eV, respectively, Table 5). The exact causes for these energy changes, however, are quite different. Upon adsorption,

NH pushes the adjacent surface Fe atoms farther apart by 0.279 Å. NH_2, however, does not create much distortion in the in-plane direction; rather, it pulls the two adjacent surface atoms upwards by 0.060 Å (Table 3). NH prefers to diffuse from one long bridge site to the adjacent one through a short bridge site. NH_2 diffuses through the following path: long bridge → hollow → short bridge. The estimated diffusion barriers for NH and NH_2 are 0.70 [0.69] eV and 0.35 [0.37] eV, respectively (Table 4).

3.2.8 Hydroxyl (OH)

The hydroxyl species can bind on either the top or hollow site of Fe(110), with the hollow site significantly more favorable (E_b = -3.81 [-3.21] eV) than the top site (E_b = -3.09 [-2.46] eV) (Table 2). In its preferred binding structure, illustrated in Figure 2, the OH species sits upright at a vertical distance of 1.311 Å above the surface, and the calculated O–H bond length is 0.981 Å (Table 3). The calculated O–H and Fe–OH stretching frequencies are 3794 cm^{-1} and 380 cm^{-1}, respectively (Table 7). The adsorption of OH results in expansion of the local Fe lattice by 0.180 Å and 0.044 Å along the long-bridge and short-bridge directions, respectively (Table 3), leading to a surface deformation energy of 0.05 [0.06] eV (Table 5). The lowest-barrier diffusion path of OH on Fe(110) is hollow → long bridge → hollow, and the estimated diffusion barrier is 0.11 [0.12] eV (Table 4).

3.2.9 Cyanide (CN)

The most stable binding structure of CN on Fe(110) is similar to that of its hydrogenated counterpart HCN: it binds through both the C and N atoms over two adjacent hollow sites across a long bridge site in the h-lb-h configuration (E_b = -5.04 [-4.40] eV) (Figure 2 and Table 2). Other less stable binding structures are also summarized in Table 2. In this h-lb-h binding geometry, the C and N atoms are located at vertical distances of 1.295 Å and 1.426 Å, respectively, above the surface; the calculated intramolecular C–N bond length is 1.260 Å (Table 3). The adsorbate-surface and intramolecular vibrational frequencies are 342 cm^{-1} and 1590 cm^{-1}, respectively (Table 7). The adsorption of CN is associated with a mild surface deformation energy of 0.05 [0.05] eV (Table 5). The diffusion behavior of CN over Fe(110) is summarized in Table 4: the estimated diffusion barrier is 0.30 [0.20] eV; along the diffusion path, the species passes through a less stable adsorption site where the C atom binds on a long bridge site, and the N atom binds on an adjacent top site.

3.2.10 COH and Formyl (HCO)

Both COH and HCO prefer to bind through the carbon atom on Fe(110). The binding energies and optimal binding structures of the two isomers are shown in Figure 2 and Table 2. COH prefers to bind on the long bridge site with a binding energy of -4.75 [-4.15] eV; it can also bind, less stably, on either the short bridge (E_b = -4.40 [-3.82] eV) or top (E_b = -3.62 [-3.10] eV) site. HCO binds the strongest with both the C and O atoms over two adjacent hollow sites across a long bridge site (the h-lb-h configuration) with a binding energy of -3.06 [-2.40] eV; a less stable t-lb-t structure also exists with a binding energy of -2.75 [-2.15] eV. When both COH and HCO are at their preferred binding sites, HCO is slightly more stable by 0.08 [0.01] eV. The detailed adsorption geometries at the preferred binding sites are summarized in Table 3. COH is adsorbed at a vertical distance of 1.150 Å above the surface; the O atom sits right above the C atom while the H atom is tilted towards the surface at an angle of 109.7º; the C–O and O–H bond lengths are 1.362 Å and 0.987 Å, respectively. When HCO is adsorbed in its preferred h-lb-h configuration, the O and C atoms are at vertical distances of 1.552 Å and 1.398 Å, above the surface; the C–O and C–H bond lengths are 1.345 Å and 1.107 Å, respectively. The calculated intramolecular stretching frequencies for COH are 1100 cm^{-1} (C–O) and 3692 cm^{-1} (O–H); those for HCO are 1127 cm^{-1} (C–O) and 2950 cm^{-1} (C–H) (Table 8). The adsorption of COH and HCO is associated with mild surface deformation energies of 0.07 [0.06] eV and 0.04 [0.05] eV, respectively (Table 5). The diffusion behavior of COH and HCO is summarized in Table 4. COH diffuses between two adjacent long bridge sites through a short bridge site with an estimated diffusion barrier of 0.35 [0.34] eV. HCO diffuses along the path h-lb-h → t-lb-t → h-lb-h with an estimated diffusion barrier of 0.31 [0.24] eV.

3.2.11 Nitrosyl Hydrides (NOH and HNO)

We calculated distinct adsorption properties for the two nitrosyl hydride species, NOH and HNO, and the results are summarized in Figure 2 and Table 2. NOH binds to Fe(110) through its nitrogen atom; the O atom sits vertically above the N atom, and the H atom is tilted towards the surface at an angle of 104.5°. We observed stable binding of NOH only on the long bridge site with a binding energy of -3.98 [-3.26] eV. On the other hand, HNO always binds through both the O and N atoms. The most stable binding structure is the one over two adjacent short bridge sites across a long bridge site, which we term as the sb-lb-sb site (E_b = -3.61 [-2.81] eV). HNO can also bind through

the h-lb-h configuration similar to the CN, HCN, and HCO species or over two adjacent top sites in the t-lb-t configuration; both binding structures are energetically less favorable by 0.41 [0.32] eV and 0.70 [0.53] eV, respectively. When both of the two isomers are adsorbed at their preferred binding sites, HNO is slightly more stable than NOH by 0.10 [0.01] eV. The detailed structural information of surface NOH and HNO at their preferred binding sites are summarized in Table 3. NOH is adsorbed at a vertical distance of 1.028 Å from the surface; the N–O and O–H bond lengths are 1.440 Å and 0.990 Å, respectively. When HNO is adsorbed at its preferred sb-lb-sb site, the O and N atoms are at vertical distances of 1.519 Å and 1.371 Å, respectively, above the surface; the intramolecular bond lengths are 1.473 Å (N–O) and 1.030 Å (N–H). The calculated intramolecular stretching frequencies of NOH are 798 cm^{-1} (N–O) and 3663 cm^{-1} (O–H); those of HNO are 667 cm^{-1} (N–O) and 3432 cm^{-1} (N–H) (Table 8). The adsorption of NOH and HNO is associated with similar deformation energy values (0.12 [0.12] eV for NOH and 0.12 [0.13] eV for HNO, Table 5); both can be attributed to the horizontal expansion of the local Fe lattice induced upon adsorption (Table 3). Table 4 shows the diffusion behavior of NOH and HNO on Fe(110): NOH diffuses along the path lb → sb → lb with an estimated energy barrier of 0.63 [0.61] eV; HNO diffuses along the path sb-lb-sb → h-lb-h → sb-lb-sb with an estimated energy barrier of 0.41 [0.31] eV.

3.3 Thermochemistry of Surface Reactions

In this section, we present the thermochemical potential energy surfaces of the decomposition reactions of NH_3, CH_4, N_2, CO, and NO over Fe(110), using the PW91 binding energy values obtained from our DFT calculations. The evaluation of the activation energy barrier for each elementary step is beyond the scope of this study. As a result, all the potential energy surfaces presented here are addressing reaction thermochemistry only. The results are summarized in Figures 4 and 5. Due to the strong binding between most adsorbates and the Fe(110) surface, all the decomposition steps are energetically downhill, and the thermochemistry always favors the completely decomposed state. Detailed results are discussed below.

We start with the decomposition of ammonia (Figure 4, black line). The decomposition process starts with the adsorption of gas-phase NH_3, which is exothermic by 0.62 eV. All of the three subsequent hydrogen-removal steps from the adsorbed NH_3* are thermodynamically favorable. The reaction energies of these three steps are -0.64 eV, -0.99 eV and -0.21 eV, in the order from the first to the third H removal, respectively. The second hydrogen removal step (NH_2* → NH* +

H*) is the most thermodynamically driven while the last one (NH* → N* + H*) is the least exothermic. The overall reaction energy for the decomposition of NH_3(g) to N* + 3H* is -2.46 eV. The decomposition process of CH_4 (Figure 4, red line) involves four exothermic hydrogen-removal steps, which leads to an overall reaction energy (CH_4(g) → C* + 4H*) of -1.60 eV. The third hydrogen-removal step (CH_2* → CH* + H*) is the most exothermic (reaction energy = -0.72 eV) while the last one is the least exothermic (reaction energy = -0.11 eV). The decomposition of N_2(g) (Figure 4, blue line) is initiated by its adsorption step, which is exothermic by -0.63 eV. The subsequent dissociation step of the adsorbed N_2* species is highly thermodynamically favorable (exothermic by -2.04 eV). The overall reaction energy of the decomposition of gas-phase N_2 to 2N* is -2.67 eV.

We now discuss the direct decomposition of CO and NO on Fe(110) (Figure 5, black and red lines). Both decomposition processes involve the adsorption of the gas-phase species and the subsequent dissociation of the adsorbed surface intermediate. The CO adsorption and CO* dissociation steps are both exothermic (by 1.91 eV and 0.76 eV, respectively), and the overall reaction energy is -2.67 eV. The NO decomposition process is even more thermodynamically driven. The NO adsorption and NO* dissociation steps are exothermic by 2.86 and 2.64 eV, which leads to an overall reaction energy of -5.50 eV. Although predictions of the reaction kinetics would require explicit calculations of the activation energy barriers, we can conclude that the complete decomposition of NH_3, CH_4, N_2, CO, and NO involves no thermochemical barriers.

The theoretical study by Ojeda et al. proposed a hydrogen-assisted pathway for the activation of CO in Fischer-Tropsch synthesis on Fe catalysts [33]. DFT calculations by Farberow et al. also suggested that the NO decomposition proceeds through a hydrogen-assisted path on Pt(111) [123]. Here we also examined the thermochemistry of the hydrogen-assisted CO (NO) decomposition paths through either COH* (NOH*) or HCO (HNO*) on Fe(110) (Figure 5, purple and blue lines). The CO decomposition process is initiated with the adsorption of CO(g) (exothermic by 1.91 eV) and the dissociative adsorption of 1/2H_2(g) (exothermic by 0.74 eV). After CO* + H* is formed on the surface, the formation of COH* and HCO* are similarly endothermic (by 0.62 eV and 0.70 eV, respectively). Both the subsequent dissociation steps of HCO* (to CH* + O*) and COH* (to C* + OH*) are exothermic. Compared to the direct dissociation of CO* to C* + O* (exothermic by -0.76 eV), the dissociation of COH* is of the same exothermicity, and that of HCO is 0.50 eV

more exothermic. Similar trends were observed for the hydrogen-assisted NO decomposition. Once NO* + H* is formed on the surface, the formation steps of both NOH* and HNO* are endothermic (by 0.44 eV and 0.34 eV, respectively). Subsequent dissociation steps of the hydrogenated intermediates are exothermic (by 2.39 and 2.77 eV for NOH* and HNO*, respectively), and the exothermicities are comparable with the direct dissociation of NO* (2.64 eV). Therefore, we conclude that, at least from the thermochemistry point of view, both H-assisted paths for CO and NO decomposition could be competitive with the direct decomposition paths on Fe(110).

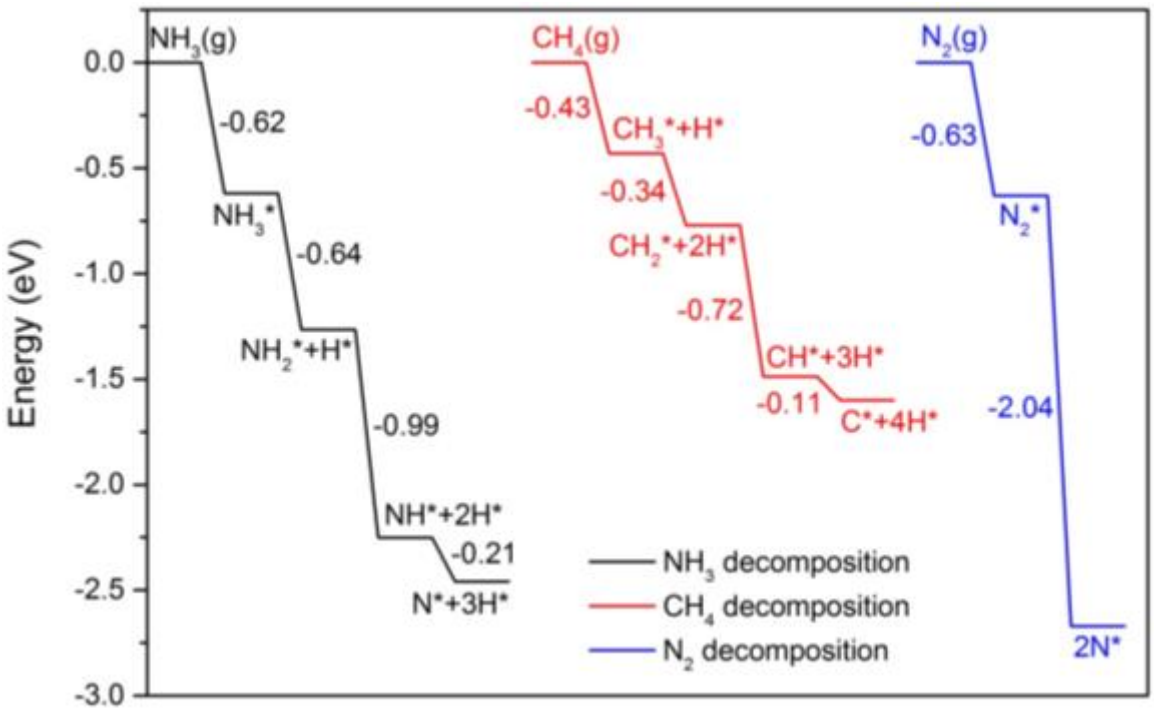

Figure 4: Thermochemistry for the direct decomposition of NH_3 (black line), CH_4 (red line) and N_2 (blue line). The reference zero corresponds to the energy of the isolated species in the gas phase and the energy of the clean Fe(110) slab at infinite separation. Energies are calculated using the PW91 functional, and each number indicates the reaction energy of the respective elementary step. Gas-phase species are indicated with (g), and adsorbed species are indicated with *. No stable binding structures were observed for CH_4, and therefore a dissociative adsorption as methyl and hydrogen is considered. The energies of states with multiple adsorbed species are calculated by assuming all the adsorbates are at infinite separation from each other.

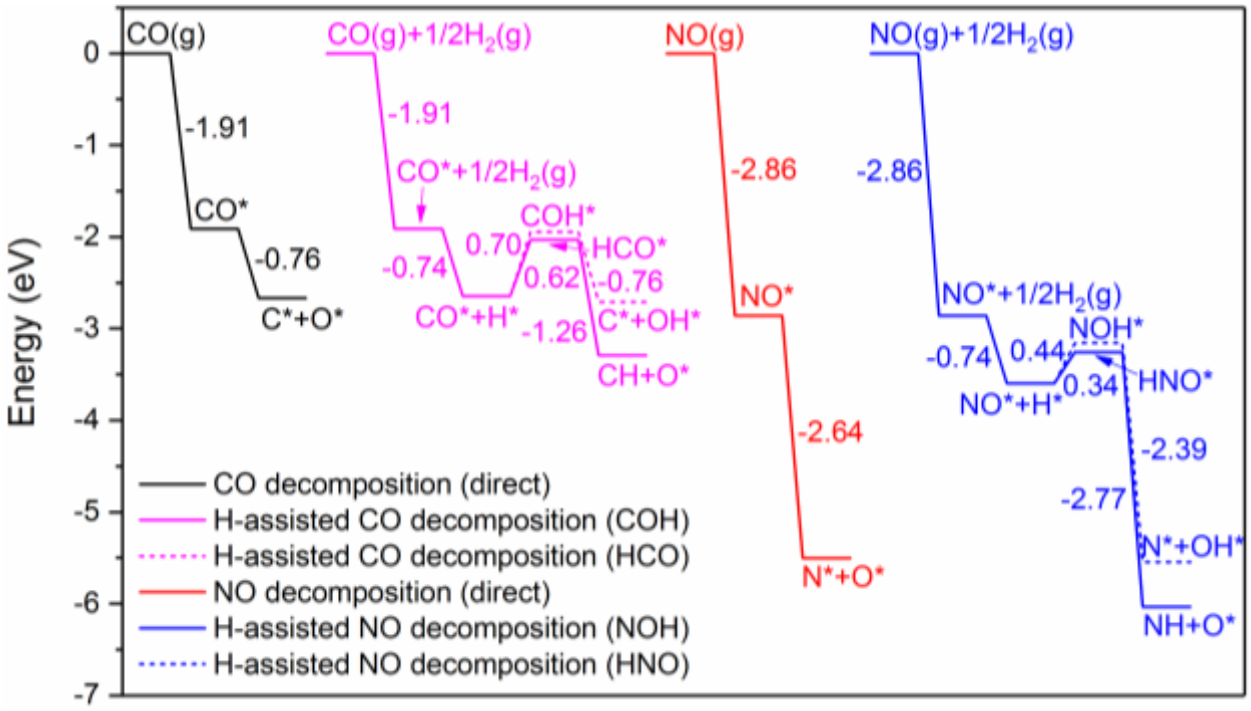

Figure 5: Thermochemistry for the direct decomposition of CO (black line) and NO (red line), as well as the hydrogen-assisted decomposition of CO (purple lines) and NO (blue lines). The reference zero corresponds to the energy of the isolated species in the gas phase and the energy of the clean Fe(110) slab at infinite separation. Energies are calculated using the PW91 functional, and each number indicates the reaction energy of the respective elementary step. Gas-phase species are indicated with (g), and adsorbed species are indicated with *. The energies of states with multiple adsorbed species are calculated by assuming all the adsorbates are at infinite separation from each other.

4. Conclusions

Using periodic, self-consistent DFT calculations, the preferred binding sites, binding energies, and the corresponding surface deformation energies of five atomic species (H, C, N, O, and S), six molecular species (NH_3, CH_4, N_2, CO, HCN, and NO), and eleven molecular fragments (CH, CH_2, CH_3, NH, NH_2, OH, CN, COH, HCO, NOH, and HNO) were determined on the Fe(110) surface at a coverage of 0.25 monolayer. No stable molecularly adsorbed structures were observed for CH_4; the binding strengths of the rest of the species calculated using the PW91 functional decreased in the following order: C > CH > N > O > S > NH > COH > CN > CH_2 > NOH > OH > HNO > HCO > NH_2 > H > NO > HCN > CH_3 > CO > N_2 > NH_3. The estimated diffusion barrier and diffusion pathway, as well as the adsorbate-surface and intramolecular vibrational modes, of all the adsorbates at their preferred binding sites were identified. Using the calculated PW91 binding energies, we studied the reaction thermochemistry of the direct decomposition of NH_3, CH_4, N_2, CO, and NO over the Fe(110) surface. All the decomposition processes are thermodynamically

downhill, and the complete decomposed states are always favored. The hydrogen-assisted paths of CO and NO decomposition were also studied; such processes give similar the reaction thermochemistry to that of the direct path. Overall, this work provides a theoretical database of the adsorption properties on Fe(110), which can be potentially valuable for future experimental and theoretical studies.

Acknowledgement

This work was supported by DOE-BES, Office of Chemical Sciences (Grant DE-FG02-05ER15731). We thank Ahmed Elnabawy and Coogan Thompson for helpful discussions. The computational work performed in this study was carried out partly through supercomputing resources from the following institutions: the National Energy Research Scientific Computing Center (NERSC); the Center for Nanoscale Materials (CNM) at Argonne National Laboratory (ANL); and the Environmental Molecular Sciences Laboratory (EMSL), a national scientific user facility at Pacific Northwest National Laboratory (PNNL). EMSL is sponsored by the Department of Energy's Office of Biological and Environmental Research located at PNNL, whereas CNM and NERSC are supported by the U.S. Department of Energy, Office of Science, under contracts DE-AC02-06CH11357 and DE-AC02-05CH11231, respectively.

References

[1] M. Boudart, Ammonia synthesis: The bellwether reaction in heterogeneous catalysis, Top. Catal. 1 (1994) 405–414. doi:10.1007/BF01492292.

[2] A. Logadottir, T.H. Rod, J.K. Nørskov, B. Hammer, S. Dahl, C.J.H. Jacobsen, The Brønsted–Evans–Polanyi relation and the volcano plot for ammonia synthesis over transition metal catalysts, J. Catal. 197 (2001) 229–231. doi:10.1006/jcat.2000.3087.

[3] A. Mittasch, W. Frankenburg, Early studies of multicomponent catalysts, Adv. Catal. 2 (1950) 81–104. doi:10.1016/S0360-0564(08)60375-2.

[4] C.J.H. Jacobsen, S. Dahl, B.G.S. Clausen, S. Bahn, A. Logadottir, J.K. Nørskov, Catalyst design by interpolation in the periodic table: Bimetallic ammonia synthesis catalysts, J. Am. Chem. Soc. 123 (2001) 8404–8405. doi:10.1021/ja010963d.

[5] A. Nielsen, An Investigation on Promoted Iron Catalysts for the Synthesis of Ammonia, Jul. Gjellerups Forlag, Copenhagen, 1968.

[6] N.D. Spencer, R.C. Schoonmaker, G.A. Somorjai, Iron single crystals as ammonia synthesis catalysts: Effect of surface structure on catalyst activity, J. Catal. 74 (1982) 129–135.

doi:10.1016/0021-9517(82)90016-1.

[7] J.A. Dumesic, H. Topsøe, M. Boudart, Surface, catalytic and magnetic properties of small iron particles. III. Nitrogen induced surface reconstruction, J. Catal. 37 (1975) 513–522. doi:10.1016/0021-9517(75)90186-4.

[8] M. Bowker, I. Parker, K.C. Waugh, The application of surface kinetic data to the industrial synthesis of ammonia, Surf. Sci. 197 (1988) L223–L229. doi:10.1016/0039-6028(88)90566-3.

[9] M. Bowker, I.B. Parker, K.C. Waugh, Extrapolation of the kinetics of model ammonia synthesis catalysts to industrially relevant temperatures and pressures, Appl. Catal. 14 (1985) 101–118. doi:10.1016/S0166-9834(00)84348-1.

[10] P. Stoltze, J.K. Nørskov, Bridging the "pressure gap" between ultrahigh-vacuum surface physics and high-pressure catalysis, Phys. Rev. Lett. 55 (1985) 2502–2505. doi:10.1103/PhysRevLett.55.2502.

[11] L.M. Aparicio, J.A. Dumesic, Ammonia synthesis kinetics: Surface chemistry, rate expressions, and kinetic analysis, Top. Catal. 1 (1994) 233–252. doi:10.1007/BF01492278.

[12] D.R. Strongin, J. Carrazza, S.R. Bare, G.A. Somorjai, The importance of C7 sites and surface roughness in the ammonia synthesis reaction over iron, J. Catal. 103 (1987) 213–215. doi:10.1016/0021-9517(87)90109-6.

[13] G. Ertl, Primary steps in catalytic synthesis of ammonia, J. Vac. Sci. Technol. A Vacuum, Surfaces, Film. 1 (1983) 1247–1253. doi:10.1116/1.572299.

[14] D.R. Strongin, G.A. Somorjai, The effects of potassium on ammonia synthesis over iron single-crystal surfaces, J. Catal. 109 (1988) 51–60. doi:10.1016/0021-9517(88)90184-4.

[15] P.H. Emmett, S. Brunauer, The adsorption of nitrogen by iron synthetic ammonia catalysts, J. Am. Chem. Soc. 56 (1934) 35–41. doi:10.1021/ja01331a507.

[16] D.R. Strongin, S.R. Bare, G.A. Somorjai, The effects of aluminum oxide in restructuring iron single crystal surfaces for ammonia synthesis, J. Catal. 103 (1987) 289–301. doi:10.1016/0021-9517(87)90121-7.

[17] M. Bowker, Nitrogen dissociation on Fe: Activated, non-activated or both?, Top. Catal. 1 (1994) 265–271. doi:10.1007/BF01492280.

[18] S. Dahl, Dissociative adsorption of dinitrogen on a multipromoted iron-based ammonia synthesis catalyst: Linking properties of catalysts and single-crystal surfaces, J. Catal. 198 (2001) 97–102. doi:10.1006/jcat.2000.3114.

[19] J.A. Dumesic, A.A. Trevino, Kinetic simulation of ammonia synthesis catalysis, J. Catal. 116 (1989) 119–129. doi:10.1016/0021-9517(89)90080-8.

[20] J. Sehested, C.J.H. Jacobsen, E. Törnqvist, S. Rokni, P. Stoltze, Ammonia synthesis over a multipromoted iron catalyst: Extended set of activity measurements, microkinetic model,

and hydrogen inhibition, J. Catal. 188 (1999) 83–89. doi:10.1006/jcat.1999.2628.

[21] G.P. Van der Laan, A.A.C.M. Beenackers, Kinetics and selectivity of the Fischer–Tropsch synthesis: A literature review, Catal. Rev. 41 (1999) 255–318. doi:10.1081/CR-100101170.

[22] M.E. Dry, The Fischer-Tropsch process: 1950-2000, Catal. Today, 2002: pp. 227–241. doi:10.1016/S0920-5861(01)00453-9.

[23] C. López, A. Corma, Supported iron nanoparticles as catalysts for sustainable production of lower olefins, ChemCatChem. 4 (2012) 751–752. doi:10.1002/cctc.201200178.

[24] J.W. Niemantsverdriet, J.W. Niemantsverdriet, A.M. Van der Kraan, A.M. Van der Kraan, W.L. Van Dijk, W.L. Van Dijk, H.S. Van der Baan, H.S. Van der Baan, Behavior of metallic iron catalysts during Fischer-Tropsch synthesis studied with Moessbauer spectroscopy, x-ray diffraction, carbon content determination, and reaction kinetic measurements, J. Phys. Chem. 84 (1980) 3363–3370. doi:10.1021/j100462a011.

[25] M.E. Dry, T. Shingles, L.J. Boshoff, G.J. Oosthuizen, Heats of chemisorption on promoted iron surfaces and the role of alkali in Fischer-Tropsch synthesis, J. Catal. 15 (1969) 190–199. doi:http://dx.doi.org/10.1016/0021-9517(69)90023-2.

[26] P. Wang, J. Kang, Q. Zhang, Y. Wang, Lithium ion-exchanged zeolite faujasite as support of iron catalyst for Fischer-Tropsch synthesis, Catal. Letters. 114 (2007) 178–184. doi:10.1007/s10562-007-9062-4.

[27] R.A. Dictor, A.T. Bell, Fischer-Tropsch synthesis over reduced and unreduced iron oxide catalysts, J. Catal. 97 (1986) 121–136. doi:10.1016/0021-9517(86)90043-6.

[28] W. Chen, Z. Fan, X. Pan, X. Bao, Effect of confinement in carbon nanotubes on the activity of Fischer-Tropsch iron catalyst, J. Am. Chem. Soc. 130 (2008) 9414–9419. doi:10.1021/ja8008192.

[29] S. Li, S. Krishnamoorthy, A. Li, G.D. Meitzner, E. Iglesia, Promoted Iron-Based Catalysts for the Fischer–Tropsch Synthesis: Design, Synthesis, Site Densities, and Catalytic Properties, J. Catal. 206 (2002) 202–217. doi:10.1006/jcat.2001.3506.

[30] M.D. Shroff, D.S. Kalakkad, K.E. Coulter, S.D. Kohler, M.S. Harrington, N.B. Jackson, A.G. Sault, A.K. Datye, Activation of Precipitated Iron Fischer-Tropsch Synthesis Catalysts, J. Catal. 156 (1995) 185–207. doi:10.1006/jcat.1995.1247.

[31] S. Li, A. Li, S. Krishnamoorthy, E. Iglesia, Effects of Zn, Cu, and K promoters on the structure and on the reduction, carburization, and catalytic behavior of iron-based Fischer-Tropsch synthesis catalysts, Catal. Letters. 77 (2001) 197–205. doi:10.1023/A:1013284217689.

[32] M. Ojeda, R. Nabar, A.U. Nilekar, A. Ishikawa, M. Mavrikakis, E. Iglesia, CO activation pathways and the mechanism of Fischer-Tropsch synthesis, J. Catal. 272 (2010) 287–297. doi:10.1016/j.jcat.2010.04.012.

[33] M. Ojeda, A. Li, R. Nabar, A.U. Nilekar, M. Mavrikakis, E. Iglesia, Kinetically relevant

steps and H_2/D_2 isotope effects in fischer-tropsch synthesis on Fe and Co catalysts, J. Phys. Chem. C. 114 (2010) 19761–19770. doi:10.1021/jp1073076.

[34] A.A. Gokhale, M. Mavrikakis, Early Fischer-Tropsch steps on Fe(110) and Co(0001) surfaces: comparative DFT studies, Prepr. Symp. - Am. Chem. Soc. Div. Fuel Chem. 50 (2005) 149–150.

[35] S.R. Kelemen, A. Kaldor, The interaction of surface sulfur with carbon on Fe(110), J. Chem. Phys. 75 (1981) 1530. doi:10.1063/1.442186.

[36] A.M. Baró, W. Erley, The chemisorption of hydrogen on a (110) iron crystal studied by vibrational spectroscopy (EELS), Surf. Sci. 112 (1981) L759–L764. doi:10.1016/0039-6028(81)90324-1.

[37] K. Yoshida, G.A. Somorjai, The chemisorption of CO, CO_2, C_2H_2, C_2H_4, H_2 and NH_3 on the clean Fe(100) and (111) crystal surfaces, Surf. Sci. 75 (1978) 46–60. doi:10.1016/0039-6028(78)90051-1.

[38] W. Nichtl-Pecher, J. Gossmann, L. Hammer, K. Heinz, K. Müller, Adsorption of hydrogen on Fe (110) at cryogenic temperatures investigated by low energy electron diffraction, J. Vac. Sci. Technol. A Vacuum, Surfaces, Film. 10 (1992) 501. doi:10.1116/1.578179.

[39] K. Yoshida, Adsorption of H_2 on (110), (111) and Stepped (111) Iron Single Crystal Surfaces, Jpn. J. Appl. Phys. 19 (1980) 1873–1883. doi:10.1143/JJAP.19.1873.

[40] W. Moritz, R. Imbihl, R.J. Behm, G. Ertl, T. Matsushima, Adsorption geometry of hydrogen on Fe(110), J. Chem. Phys. 83 (1985) 1959–1968. doi:doi:http://dx.doi.org/10.1063/1.449334.

[41] L. Hammer, H. Landskron, W. Nichtl-Pecher, A. Fricke, K. Heinz, K. Müller, Hydrogen-induced restructuring of close-packed metal surfaces: H/Ni(111) and H/Fe(110), Phys. Rev. B. 47 (1993) 15969–15972. doi:10.1103/PhysRevB.47.15969.

[42] F. Bozso, G. Ertl, M. Grunze, M. Weiss, Chemisorption of hydrogen on iron surfaces, Appl. Surf. Sci. 1 (1977) 103–119. doi:10.1016/0378-5963(77)90009-5.

[43] R. Imbihl, R.J. Behm, K. Christmann, G. Ertl, T. Matsushima, Phase transitions of a two-dimensional chemisorbed system: H on Fe(110), Surf. Sci. 117 (1982) 257–266. doi:10.1016/0039-6028(82)90506-4.

[44] E.A. Kurz, J.B. Hudson, The adsorption of H_2 and D_2 on Fe(110), Surf. Sci. 195 (1988) 31–42. doi:10.1016/0039-6028(88)90778-9.

[45] A. Juan, R. Hoffmann, Hydrogen on the Fe(110) surface and near bulk bcc Fe vacancies, Surf. Sci. 421 (1999) 1–16. doi:10.1016/S0039-6028(98)00780-8.

[46] W. Xie, L. Peng, D. Peng, F.L. Gu, J. Liu, Processes of H_2 adsorption on Fe(110) surface: A density functional theory study, Appl. Surf. Sci. 296 (2014) 47–52. doi:10.1016/j.apsusc.2014.01.028.

[47] D.E. Jiang, E.A. Carter, Adsorption and diffusion energetics of hydrogen atoms on Fe(110) from first principles, Surf. Sci. 547 (2003) 95–98. doi:10.1016/j.susc.2003.10.007.

[48] G. Brodén, G. Gafner, H.P. Bonzel, A UPS and LEED/Auger study of adsorbates on Fe(110), Appl. Phys. 13 (1977) 333–342. doi:10.1007/BF00882607.

[49] F. Bozso, G. Ertl, M. Weiss, Interaction of nitrogen with iron surfaces. II. Fe(110), J. Catal. 50 (1977) 519–529. doi:10.1016/0021-9517(77)90063-X.

[50] J.J.F. Scholten, P. Zwietering, J.A. Konvalinka, J.H. de Boer, Chemisorption of nitrogen on iron catalysts in connection with ammonia synthesis. Part 1. The kinetics of the adsorption and desorption of nitrogen, Trans. Faraday Soc. 55 (1959) 2166. doi:10.1039/tf9595502166.

[51] V. PONEC, Z. Knor, On the forms of nitrogen adsorbed on iron, J. Catal. 10 (1968) 73–82. doi:10.1016/0021-9517(68)90225-X.

[52] J. Böheim, W. Brenig, T. Engel, U. Leuthäusser, Kinetics of nitrogen adsorption on iron, Surf. Sci. 131 (1983) 258–272. doi:10.1016/0039-6028(83)90276-5.

[53] Š. Pick, P. Légaré, C. Demangeat, Density-functional study of the chemisorption of N on and below Fe(110) and Fe(001) surfaces, Phys. Rev. B - Condens. Matter Mater. Phys. 75 (2007) 195446. doi:10.1103/PhysRevB.75.195446.

[54] J.J. Mortensen, M.V. Ganduglia-Pirovano, L.B. Hansen, B. Hammer, P. Stoltze, J.K. Nørskov, Nitrogen adsorption on Fe(111), (100), and (110) surfaces, Surf. Sci. 422 (1999) 8–16. doi:10.1016/S0039-6028(98)00802-4.

[55] T. Wang, X. Tian, Y. Yang, Y.W. Li, J. Wang, M. Beller, H. Jiao, Coverage-dependent N_2 adsorption and its modification of iron surfaces structures, J. Phys. Chem. C. 120 (2016) 2846–2854. doi:10.1021/acs.jpcc.5b11953.

[56] C. Leygraf, S. Ekelund, A LEED-AES study of the oxidation of Fe(110) and Fe(100), Surf. Sci. 40 (1973) 609–635. doi:10.1016/0039-6028(73)90148-9.

[57] A. Wight, N.G. Condon, F.M. Leibsle, G. Worthy, A. Hodgson, Intitial stages of Fe(110) oxidation at 300 K: Kinetic and structure, Surf. Sci. 331–333 (1995) 133–137. doi:10.1016/0039-6028(95)00176-X.

[58] A.J. Pignocco, G.E. Pellissier, LEED studies of oxygen adsorption and oxide formation on an (011) iron surface, Surf. Sci. 7 (1967) 261–278. doi:10.1016/0039-6028(67)90020-9.

[59] A.J. Melmed, J.J. Carroll, Oxidation of (011) Iron at room temperature: Mainly LEED aspects, J. Vac. Sci. Technol. 10 (1973) 164. doi:10.1116/1.1317930.

[60] H.-J. Kim, E. Vescovo, Spin-resolved photoemission investigation of the c(2×2) and c(3×1) oxygen overlayers on the Fe(110) surface, Phys. Rev. B. 58 (1998) 14047–14050. doi:10.1103/PhysRevB.58.14047.

[61] W. Erley, H. Ibach, Vibrational excitations and structure of oxygen on Fe(110), Solid State Commun. 37 (1981) 937–942. doi:10.1016/0038-1098(81)91190-X.

[62] G. Pirug, G. Brodén, H.P. Bonzel, Coadsorption of potassium and oxygen on Fe(110), Surf. Sci. 94 (1980) 323–338. doi:10.1016/0039-6028(80)90010-2.

[63] H.-J. Kim, J.-H. Park, E. Vescovo, Oxidation of the Fe(110) surface: An Fe_3O_4(111) / Fe(110) bilayer, Phys. Rev. B. 61 (2000) 15284–15287. doi:10.1103/PhysRevB.61.15284.

[64] J. Weissenrieder, M. Göthelid, M. Månsson, H. Von Schenck, O. Tjernberg, U.O. Karlsson, Oxygen structures on Fe(110), Surf. Sci. 527 (2003) 163–172. doi:10.1016/S0039-6028(03)00018-9.

[65] Y. Sakisaka, T. Komeda, T. Miyano, M. Onchi, S. Masuda, Y. Harada, K. Yagi, H. Kato, Angle-resolved photoemission of the c(2×2) and c(3×1) oxygen overlayers on Fe(110), Surf. Sci. 164 (1985) 220–234. doi:10.1016/0039-6028(85)90709-5.

[66] E. Vescovo, C. Carbone, W. Eberhardt, O. Rader, T. Kachel, W. Gudat, Spin-resolved photoemission study of the clean and oxygen-covered Fe(110) surface, Phys. Rev. B. 48 (1993) 285–288. doi:10.1103/PhysRevB.48.285.

[67] M. Eder, K. Terakura, J. Hafner, Initial stages of oxidation of (100) and (110) surfaces of iron caused by water, Phys. Rev. B. 64 (2001) 115426. doi:10.1103/PhysRevB.64.115426.

[68] P. Błoński, A. Kiejna, J. Hafner, Theoretical study of oxygen adsorption at the Fe(110) and (100) surfaces, Surf. Sci. 590 (2005) 88–100. doi:10.1016/j.susc.2005.06.011.

[69] T. Ossowski, A. Kiejna, Oxygen adsorption on Fe(110) surface revisited, Surf. Sci. 637–638 (2015) 35–41. doi:10.1016/j.susc.2015.03.001.

[70] D.H. Buckley, Adhesion of metals to a clean iron surface studied with LEED and auger emission spectroscopy, Wear. 20 (1972) 89–103. doi:10.1016/0043-1648(72)90290-6.

[71] W. Arabczyk, E. Rausche, Model cluster studies of the restructuring of the Fe(110) surface induced by the adsorption of carbon, nitrogen or oxygen, Pol. J. Chem. 70 (1996).

[72] D.E. Jiang, E.A. Carter, Carbon atom adsorption on and diffusion into Fe(110) and Fe(100) from first principles, Phys. Rev. B - Condens. Matter Mater. Phys. 71 (2005) 45402. doi:10.1103/PhysRevB.71.045402.

[73] S. Riikonen, A. V. Krasheninnikov, R.M. Nieminen, Submonolayers of carbon on α-Fe facets: An ab initio study, Phys. Rev. B - Condens. Matter Mater. Phys. 82 (2010) 125459. doi:10.1103/PhysRevB.82.125459.

[74] J. Weissenrieder, M. Göthelid, G. Le Lay, U.O. Karlsson, Investigation of the surface phase diagram of Fe(110)–S, Surf. Sci. 515 (2002) 135–142. doi:10.1016/S0039-6028(02)01848-4.

[75] H.D. Shih, F. Jona, D.W. Jepsen, P.M. Marcus, Metal-surface reconstruction induced by adsorbate: Fe(110) p(2×2)-S, Phys. Rev. Lett. 46 (1981) 731–734. doi:10.1103/PhysRevLett.46.731.

[76] J. Oudar, Structural study of the adsorption of sulfur on different metals, Bull. La Soc. Fr.

Mineral. Cristallogr. 94 (1971) 225–234.

[77] M.J.S. Spencer, I.K. Snook, I. Yarovsky, Effect of S arrangement on Fe(110) properties at 1/3 monolayer coverage: A DFT study, J. Phys. Chem. B. 110 (2006) 956–962. doi:10.1021/jp054769f.

[78] M.J.S. Spencer, I.K. Snook, I. Yarovsky, Coverage-dependent adsorption of atomic sulfur on Fe(110): A DFT study, J. Phys. Chem. B. 109 (2005) 9604–9612. doi:10.1021/jp0443781.

[79] M. Drechsler, H. Hoinkes, H. Kaarmann, H. Wilsch, G. Ertl, M. Weiss, Interaction of NH3 with Fe(110): Identification of surface species by means of Secondary Ion Mass Spectroscopy (SIMS), Appl. Surf. Sci. 3 (1979) 217–228. doi:10.1016/0378-5963(79)90021-7.

[80] M. Weiss, G. Ertl, F. Nitschké, Adsorption and decomposition of ammonia on Fe(110), Appl. Surf. Sci. 2 (1979) 614–635. doi:10.1016/0378-5963(79)90049-7.

[81] J.P. Toennies, C. Wöll, G. Zhang, Low-energy vibrations of NH_3 and CO adsorbed on Fe(110), J. Chem. Phys. 96 (1992) 4023. doi:10.1063/1.461852.

[82] A.K. Bhattacharya, M.A. Chesters, An Auger electron spectroscopic study of the reaction ammonia with Fe(110), J. Catal. 108 (1987) 484. doi:10.1016/0021-9517(87)90196-5.

[83] W. Erley, H. Ibach, Vibrational spectra of ammonia adsorbed on Fe(110), Surf. Sci. 119 (1982) L357–L362. doi:10.1016/0039-6028(82)90180-7.

[84] W. Erley, H. Ibach, The adsorption of ammonia on an Fe(110) single-crystal surface studied by high-resolution electron energy-loss spectroscopy (eels), J. Electron Spectros. Relat. Phenomena. 31 (1983) 161–174. doi:10.1016/0368-2048(83)80019-X.

[85] S. Satoh, H. Fujimoto, H. Kobayashi, Theoretical study of NH_3 adsorption on Fe(110) and Fe(111) surfaces, J. Phys. Chem. B. 110 (2006) 4846–4852. doi:10.1021/jp055097w.

[86] G. Gafner, R. Feder, A low-energy electron diffraction study of Fe(110): I. Experimental, Surf. Sci. 57 (1976) 37–44. doi:10.1016/0039-6028(76)90165-5.

[87] G. Brodén, G. Gafner, H.P. Bonzel, CO adsorption on potassium promoted Fe(110), Surf. Sci. 84 (1979) 295–314. doi:10.1016/0039-6028(79)90139-0.

[88] W. Erley, Vibrational spectra of CO chemisorbed on Fe (110), J. Vac. Sci. Technol. 18 (1981) 472. doi:10.1116/1.570768.

[89] R. Feder, G. Gafner, A low-energy electron diffraction study of Fe(110) : II. Theory and comparison with the experiment, Surf. Sci. 57 (1976) 45–52. doi:10.1016/0039-6028(76)90166-7.

[90] G. Wedler, H. Ruhmann, Laser induced thermal desorption of carbon monoxide from Fe(110) surfaces, Surf. Sci. 121 (1982) 464–486. doi:10.1016/0039-6028(82)90255-2.

[91] L. Gonzalez, R. Miranda, S. Ferrer, A thermal desorption study of the adsorption of CO on

Fe(110); enhancement of dissociation by surface defects, Surf. Sci. 119 (1982) 61–70. doi:10.1016/0039-6028(82)90187-X.

[92] T. Maruyama, Y. Sakisaka, H. Kato, Y. Aiura, H. Yanashima, CO on Fe(110): an angle-resolved photoemission study, Surf. Sci. 304 (1994) 281–290. doi:10.1016/0039-6028(94)91338-2.

[93] G. Ertl, J. Küppers, F. Nitschke, M. Weiss, Photoelectron spectroscopic study of surface complexes on Fe(110), Chem. Phys. Lett. 52 (1977) 309–313. doi:10.1016/0009-2614(77)80548-4.

[94] G. Wedler, R. Ruhmann, Study of the adsorption and decomposition of CO on Fe(110) with an improved vibrating capacitor, Appl. Surf. Sci. 14 (1983) 137–148. doi:10.1016/0378-5963(83)90092-2.

[95] E.S. Jensen, C.W. Seabury, T.N. Rhodin, Angle-resolved photoemission from CO on Fe(110), Solid State Commun. 35 (1980) 581–585. doi:10.1016/0038-1098(80)90587-6.

[96] A. Chakrabarty, O. Bouhali, N. Mousseau, C.S. Becquart, F. El-Mellouhi, Insights on finite size effects in ab initio study of CO adsorption and dissociation on Fe 110 surface, J. Appl. Phys. 120 (2016) 55301. doi:10.1063/1.4959990.

[97] A. Stibor, G. Kresse, A. Eichler, J. Hafner, Density functional study of the adsorption of CO on Fe(1 1 0), in: Surf. Sci., 2002: pp. 99–102. doi:10.1016/S0039-6028(02)01182-2.

[98] A. Chakrabarty, O. Bouhali, N. Mousseau, C.S. Becquart, F. El-Mellouhi, Insights on finite size effects in ab initio study of CO adsorption and dissociation on Fe 110 surface, J. Appl. Phys. 120 (2016) 55301. doi:10.1063/1.4959990.

[99] T. Wang, X.X. Tian, Y.W. Li, J. Wang, M. Beller, H. Jiao, Coverage-dependent CO adsorption and dissociation mechanisms on iron surfaces from DFT computations, ACS Catal. 4 (2014) 1991–2005. doi:10.1021/cs500287r.

[100] M. Mavrikakis, J. Rempel, J. Greeley, L.B. Hansen, J.K. Nørskov, Atomic and molecular adsorption on Rh(111), J. Chem. Phys. 117 (2002) 6737–6744. doi:10.1063/1.1507104.

[101] W.P. Krekelberg, J. Greeley, M. Mavrikakis, Atomic and Molecular Adsorption on Ir(111), J. Phys. Chem. B. 108 (2004) 987–994. doi:10.1021/jp035786c.

[102] D.C. Ford, Y. Xu, M. Mavrikakis, Atomic and molecular adsorption on Pt(1 1 1), Surf. Sci. 587 (2005) 159–174. doi:10.1016/j.susc.2005.04.028.

[103] J.A. Herron, S. Tonelli, M. Mavrikakis, Atomic and molecular adsorption on Pd(111), Surf. Sci. 606 (2012) 1670–1679. doi:10.1016/j.susc.2012.07.003.

[104] J.A. Herron, S. Tonelli, M. Mavrikakis, Atomic and molecular adsorption on Ru(0001), Surf. Sci. 614 (2013) 64–74. doi:10.1016/j.susc.2013.04.002.

[105] K. Hahn, M. Mavrikakis, Atomic and molecular adsorption on Re(0001), Top. Catal. 57 (2014) 54–68. doi:10.1007/s11244-013-0162-7.

[106] Y. Santiago-Rodríguez, J.A. Herron, M.C. Curet-Arana, M. Mavrikakis, Atomic and molecular adsorption on Au(111), Surf. Sci. 627 (2014) 57–69. doi:10.1016/j.susc.2014.04.012.

[107] M.C. Crowe, C.T. Campbell, Adsorption microcalorimetry: Recent advances in instrumentation and application., Annu. Rev. Anal. Chem. 4 (2011) 41–58. doi:10.1146/annurev-anchem-061010-113841.

[108] C.E. Borroni-Bird, N. Al-Sarraf, S. Andersoon, D.A. King, Single crystal adsorption microcalorimetry, Chem. Phys. Lett. 183 (1991) 516–520. doi:10.1016/0009-2614(91)80168-W.

[109] J.S. Hummelshøj, F. Abild-Pedersen, F. Studt, T. Bligaard, J.K. Nørskov, CatApp: A web application for surface chemistry and heterogeneous catalysis, Angew. Chemie - Int. Ed. 51 (2012) 272–274. doi:10.1002/anie.201107947.

[110] B. Hammer, L.B. Hansen, J.K. Nørskov, Improved adsorption energetics within density-functional theory using revised Perdew-Burke-Ernzerhof functionals, Phys. Rev. B. 59 (1999) 7413–7421. doi:10.1103/PhysRevB.59.7413.

[111] J. Greeley, J.K. Nørskov, M. Mavrikakis, Electronic structure and catalysis on metal surfaces, Annu. Rev. Phys. Chem. 53 (2002) 319–348. doi:10.1146/annurev.physchem.53.100301.131630.

[112] D. Vanderbilt, Soft self-consistent pseudopotentials in a generalized eigenvalue formalism, Phys. Rev. B. 41 (1990) 7892–7895. doi:10.1103/PhysRevB.41.7892.

[113] J.P. Perdew, J.A. Chevary, S.H. Vosko, K.A. Jackson, M.R. Pederson, D.J. Singh, C. Fiolhais, Atoms, molecules, solids, and surfaces: Applications of the generalized gradient approximation for exchange and correlation, Phys. Rev. B. 46 (1992) 6671–6687. doi:10.1103/PhysRevB.46.6671.

[114] G. Kresse, J. Furthmüller, Efficiency of ab-initio total energy calculations for metals and semiconductors using a plane-wave basis set, Comput. Mater. Sci. 6 (1996) 15–50. doi:10.1016/0927-0256(96)00008-0.

[115] H. Monkhorst, J. Pack, Special points for Brillouin-zone integrations, Phys. Rev. B. 13 (1976) 5188–5192. doi:10.1103/PhysRevB.13.5188.

[116] J. Neugebauer, M. Scheffler, Adsorbate-substrate and adsorbate-adsorbate interactions of Na and K adlayers on Al (111), Phys. Rev. B. 46 (1992) 16067–16080. doi:10.1103/PhysRevB.46.16067.

[117] L. Bengtsson, Dipole correction for surface supercell calculations, Phys. Rev. B. 59 (1999) 12301–12304. doi:10.1103/PhysRevB.59.12301.

[118] V. Milman, B. Winkler, J.A. White, C.J. Pickard, M.C. Payne, E. V. Akhmatskaya, R.H. Nobes, Electronic structure, properties, and phase stability of inorganic crystals: A pseudopotential plane-wave study, Int. J. Quantum Chem. 77 (2000) 895–910. doi:10.1002/(SICI)1097-461X(2000)77:5<895::AID-QUA10>3.0.CO;2-C.

[119] J. Greeley, M. Mavrikakis, A first-principles study of surface and subsurface H on and in Ni(111): Diffusional properties and coverage-dependent behavior, Surf. Sci. 540 (2003) 215–229. doi:10.1016/S0039-6028(03)00790-8.

[120] I.H. Sahputra, A. Chakrabarty, O. Restrepo, O. Bouhali, N. Mousseau, C.S. Becquart, F. El-Mellouhi, Carbon adsorption on and diffusion through the Fe(110) surface and in bulk: Developing a new strategy for the use of empirical potentials in complex material set-ups, Phys. Status Solidi B 254 (2017) 1600408. doi: 10.1002/pssb.201600408.

[121] P.J. Feibelman, B. Hammer, J.K. Nørskov, F. Wagner, M. Scheffler, R. Stumpf, R. Watwe, J. Dumesic, The CO/Pt(111) Puzzle, J. Phys. Chem. B. 105 (2001) 4018–4025. doi:10.1021/jp002302t.

[122] M. Gajdos, J. Hafner, CO adsorption on Cu(111) and Cu(001) surfaces: Improving site preference in DFT calculations, Surf. Sci. 590 (2004) 117–126. doi:10.1016/j.susc.2005.04.047.

[123] C.A. Farberow, J.A. Dumesic, M. Mavrikakis, Density functional theory calculations and analysis of reaction pathways for reduction of nitric oxide by hydrogen on Pt(111), ACS Catal. 4 (2014) 3307–3319. doi:10.1021/cs500668k.